Research Article | Vol. 25, No. 10 | 15 May 2017 | OPTICS EXPRESS 11827
Optics EXPRESS

Continuous-wave and SESAM mode-locked femtosecond operation of a Yb:$MgWO_4$ laser

HAIFENG LIN,[1] GE ZHANG,[1] LIZHEN ZHANG,[1] ZHOUBIN LIN,[1] FEDERICO PIRZIO,[2,*] ANTONIO AGNESI,[2] VALENTIN PETROV,[3] AND WEIDONG CHEN[1,3,4]

[1]*Key Laboratory of Optoelectronic Materials Chemistry and Physics, Fujian Institute of Research on the Structure of Matter, Chinese Academy of Sciences, Fuzhou, Fujian 350002, China*
[2]*Universita' di Pavia, Dip. Ing. Industriale e dell'Informazione, Via Ferrata 5, 27100 Pavia, Italy*
[3]*Max-Born-Institute for Nonlinear Optics and Ultrafast Spectroscopy, 2A Max-Born-Str., D-12489 Berlin, Germany*
[4]*chenweidong@fjirsm.ac.cn*
[*]*federico.pirzio@unipv.it*

Abstract: We present a detailed continuous-wave regime characterization and, for the first time to the best of our knowledge, SESAM mode-locked femtosecond operation with a monoclinic, Yb^{3+}-doped, $MgWO_4$ crystal. Pumping with a low-power, single-mode fiber-coupled laser diode emitting at 976 nm, we demonstrate threshold for continuous-wave (cw) operation as low as 50 mW (absorbed pump power) and slope efficiency up to ~60% (with respect to the absorbed pump power) for two of the principal emission polarizations. The output wavelength in the cw regime is continuously tunable over a ~50 nm broad range. Mode-locking the laser with a SESAM, we achieve almost Fourier-transform limited pulses with a duration of 132 and 125 fs depending on the polarization.

OCIS codes: (140.3615) Lasers, ytterbium; (140.7090) Ultrafast lasers.

References and links

1. V. B. Kravchenko, "Crystal structure of the monoclinic form of magnesium tungstate $MgWO_4$," J. Struct. Chem. **10**, 139–140 (1969).
2. E. Cavalli, A. Belletti, and M. G. Brik, "Optical spectra and energy levels of the Cr^{3+} ions in MWO_4 (M = Mg, Zn, Cd) and $MgMoO_4$ crystals," J. Phys. Chem. Solids **69**, 29–34 (2008).
3. L. Zhang, Y. Huang, S. Sun, F. Yuan, Z. Lin, and G. Wang, "Thermal and spectral characterization of Cr^{3+}:$MgWO_4$ – a promising tunable laser material," J. Lumin. **169**, Part A, 161–164 (2016).
4. R. L. Aggarwal, D. J. Ripin, J. R. Ochoa, and T. Y. Fan,"Measurement of thermo-optic properties of $Y_3Al_5O_{12}$, $Lu_3Al_5O_{12}$, $YAIO_3$, $LiYF_4$, $LiLuF_4$, BaY_2F_8, $KGd(WO_4)_2$, and $KY(WO_4)_2$ laser crystals in the 80-300K temperature range," Journal of Applied Physics **98**, 103514 (2005).
5. V. Petrov, M. C. Pujol, X. Mateos, O. Silvestre, S. Rivier, M. Aguilo, R. M. Sole, J. Liu, U. Griebner, F. Diaz, "Growth and properties of $KLu(WO_4)_2$, and novel ytterbium and thulium lasers based on this monoclinic crystalline host," Laser Photon. Rev. **1**, 179–212 (2007).
6. L. Zhang, W. Chen, J. Lu, H. Lin, L. Li, G. Wang, G. Zhang, and Z. Lin, "Characterization of growth, optical properties, and laser performance of monoclinic Yb:$MgWO_4$ crystal," Opt. Mater. Express **6**, 1627–1634 (2016).
7. N. V. Kuleshov, A. A. Lagatsky, V. G. Shcherbitsky, V. P. Mikhailov, E. Heumann, T. Jensen, A. Diening, and G. Huber, "CW laser performance of Yb and Er, Yb doped tungstates," Appl. Phys. B **64**, 409–413 (1997).
8. L. Zhang, H. Lin, G. Zhang, X. Mateos, J. M. Serres, M. Aguilo, F. Diaz, U. Griebner, V. Petrov, Y. Wang, P. Loiko, E. Vilejshikova, K. Yumashev, Z. Lin, W. Chen, "Crystal growth, optical spectroscopy and laser action of Tm^{3+}-doped monoclinic magnesium tungstate," Opt. Express **25**, 3682–3693 (2017).
9. K. Beil, S. T. Fredrich-Thornton, F. Tellkamp, R. Peters, C. Kr'ankel, K. Petermann, and G. Huber, "Thermal and laser properties of Yb:LuAG for kW thin disk lasers," Opt. Express **18**, 20712–20722 (2010).
10. F. Pirzio, M. Kemnitzer, A. Guandalini, F. Kienle, S. Veronesi, M. Tonelli, J. Aus der Au, and A. Agnesi, "Ultrafast, solid-state oscillators based on broadband, multisite Yb-doped crystals," Opt. Express **24**, 11782–11792 (2016).
11. J. A. Caird, S. A. Payne, P. R. Staber, A. J. Ramponi, L. L. Chase, and W. F. Krupke, "Quantum electronic properties of the $Na_3Ga_2Li_3F_{12}$:Cr^{3+} laser," IEEE J. Quantum Electron. **24**, 1077–1099 (1988).
12. D. Kopf, G. J. Spühler, K. J. Weingarten, and U. Keller, "Mode-locked laser cavities with a single prism for dispersion compensation," Appl. Opt. **35**, 912–915 (1996).

#291548 https://doi.org/10.1364/OE.25.011827
Journal © 2017 Received 30 Mar 2017; revised 2 May 2017; accepted 2 May 2017; published 10 May 2017
Corrected: 19 May 2017

Optics EXPRESS

1. Introduction

Magnesium tungstate ($MgWO_4$) belongs to the crystal family of monoclinic (space group $P2/c$), divalent metal mono-tungstates, having the general chemical formula MWO_4 where M = Mg, Mn, Ni, Cd or Zn [1, 2]. It shows a rather high thermal conductivity of ~8.7 W/mK [3]. This value is almost three times higher compared to the monoclinic potassium double tungstates, $KRE(WO_4)_2$ [4, 5], and even higher compared to the tetragonal sodium or lithium double tungstates $NaRE(WO_4)_2$ / $LiRE(WO_4)_2$ where RE denotes a "passive" rare earth element. The difference in ionic radius between the divalent Mg^{2+} and trivalent Yb^{3+} ions induces distortion of the crystal field. This leads to a broadening of the absorption and emission bands, which relaxes the pump wavelength stability requirements, and favors high power applications and broadly tunable operation at ~1 μm [6]. For instance, if compared to $Yb:KRE(WO_4)_2$ [5, 7], $Yb:MgWO_4$ shows an almost two-times broader absorption peak with a full-width half-maximum (FWHM) of ~7 nm, centered at 975 nm [6].

The first laser operation of Yb^{3+}- and Tm^{3+}-doped $MgWO_4$ crystals was reported only very recently [6, 8]. By pumping with a multi-mode, multi-Watt fiber coupled laser diode at 975 nm, the cw $Yb:MgWO_4$ laser generated an output power as high as 2.5 W, with a slope efficiency ≈53%, in a two-mirror, plano-convex resonator sustaining multiple transverse mode oscillation [8].

In this work we present a detailed cw and mode-locking (ML) characterization of a $Yb:MgWO_4$ laser. To this purpose, we decided to exploit low-power, single-mode diode pumping [10], in order to investigate the laser material performance with no additional thermal issues that would complicate the interpretation of the results. For the first time to the best of our knowledge, we demonstrate stable and self-starting ML in the soliton regime, employing a semiconductor saturable absorber mirror (SESAM). Pulses of ~130-fs duration with ~12 nm FWHM optical spectrum centered at 1065 nm are obtained.

2. Experimental setup and results

The X-folded resonator layout for cw and soliton ML experiments is shown in Fig. 1.

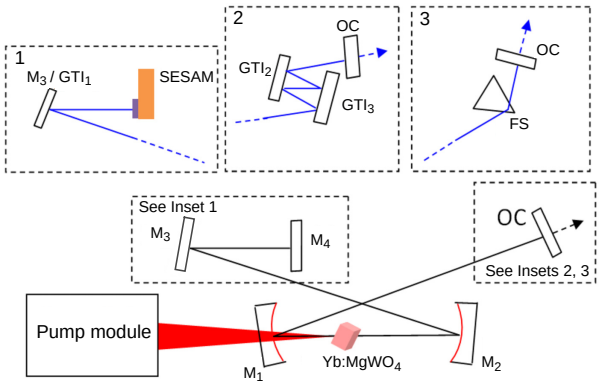

Fig. 1. Setup for the cw laser and (insets) ML experiments. M_1: spherical pump mirror (R = 50 mm), anti-reflection (AR) coated at 976 nm, highly-reflective (HR) at 1000-1100 nm; M_2: spherical mirror (R = 100 mm), HR at 1000-1100 nm; M_3: plane mirror AR coated at 976 nm and HR at 1000-1100 nm, M_4: plane mirror HR at 1000-1100 nm. SESAM: semiconductor saturable absorber mirror; GTI: Gires-Tournois interferometer mirrors: GTI_1, GTI_3 = -550 fs^2, GTI_2 = -375 fs^2; FS: fused silica dispersive Brewster prism; OC: output coupler, 30' wedged.

Optics EXPRESS

The pump-diode module consisted of a single transverse-mode, fiber-coupled laser diode (JDSU S27-7602-400) emitting at 976 nm. The laser diode output beam was not polarized, but by properly coiling the fiber pig-tail we were able to induce a strongly elliptical polarization with a ratio of about 13:1 between the two axes. The laser diode beam was collimated by means of an aspherical lens (f = 15.3 mm, NA = 0.16) and focused into the laser crystal with a Gaussian waist radius of 12 μm by using a spherical lens with 50 mm focal length. The maximum incident pump power was 375 mW.

The active medium was a 3 × 3 × 3 mm^3, Yb-doped $MgWO_4$ crystal; the dopant ion concentration was $n_{tot} = 1.819 \cdot 10^{20}$ cm^{-3}, corresponding to 1.25-at.%. Details about the crystal growth and the spectroscopic characterization can be found in [6]. In Table 1, we summarize the more relevant spectroscopic and thermo-optical properties of Yb:$MgWO_4$ and, for comparison, Yb:$KY(WO_4)_2$ and Yb:YAG.

Table 1. More relevant spectroscopic and thermo-optical properties of Yb:$MgWO_4$ (from [3, 6]). For comparison same data are reported for Yb:$KY(WO_4)_2$ (from [4]) and Yb:YAG (from [9]).

	Yb:$MgWO_4$ $E_L \parallel X$	Yb:$MgWO_4$ $E_L \parallel Y$	Yb:$KY(WO_4)_2$	Yb:YAG
λ_p [nm]	975	975	981	941, 968
σ_{ab}^{peak} [$\cdot 10^{-20}$ cm^2]	3.76	2.43	2.7 ($\parallel N_p$)	0.82
$\Delta\lambda_p$ [nm]	7.1	7.1	3.7	18, 3
τ_f [μs]	366	366	300	1200
k [W/(mK)]	8.7	8.7	2.7	$\simeq 9$

During laser experiments, the sample was placed on a metallic plate and oriented at Brewster-angle for minimization of insertion losses. Resonator curved mirror folding angles were optimized in order to compensate the cavity mode astigmatism in the active medium. In both cw and ML operation, we exploited the resonator stability region corresponding to a larger separation M_1-M_2. Therefore, we could control the cavity mode waist on mirror M_4/SESAM by properly adjusting the distance M_2-M_4 and M_1-M_2 separation.

Through ABCD modeling of the resonator, we could estimate a fundamental cavity mode dimension (waist radius) in the active medium ranging from $w_g = 12$ to 15 μm within the stability region, depending on the total resonator length.

2.1. Continuous-wave operation

We preliminarily tested the crystal in cw regime for both possible orientations, with laser emission polarization parallel to crystal X-axis ($E_L \parallel X$) or Y-axis ($E_L \parallel Y$). Note that XYZ denote the dielectric frame of the monoclinic $MgWO_4$ but the principal values of the refractive index are still unknown – thus the chosen notation serves just to establish a correspondence between the laser results and the frame in which the spectroscopic properties were characterized [6]. The gain cross section calculated for both orientations for different values of the inversion ratio $\beta = \frac{n_2}{n_{tot}}$ [10] in the range of values typical for low loss/low output coupling femtosecond oscillators, are shown in Fig. 2. As it can be seen, the $E_L \parallel Y$ crystal orientation presents a higher peak value and slightly broader gain cross section spectrum. Nevertheless, both crystal orientations ensure a broad gain spectrum suitable for femtosecond pulse generation.

Referring to Fig. 1, in the cw regime, the cavity arm lengths were set as follows: M_2-M_4 = 200 mm; M_1-M_2 = 94 mm; and M_1-OC = 450 mm. In this configuration, from ABCD modeling

Optics EXPRESS

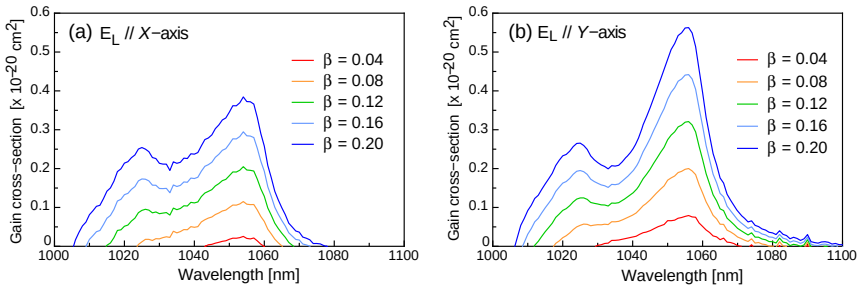

Fig. 2. Gain cross-section spectra of Yb:MgWO4 as a function of the inversion factor β for: (a) polarization along X-axis and (b) polarization along Y-axis.

of the resonator fundamental cavity mode, we expected a beam waist in the active medium $w_g \simeq 13\ \mu$m. The results obtained in the cw regime with a set of output couplers (OCs) with different transmission are shown in Fig. 3.

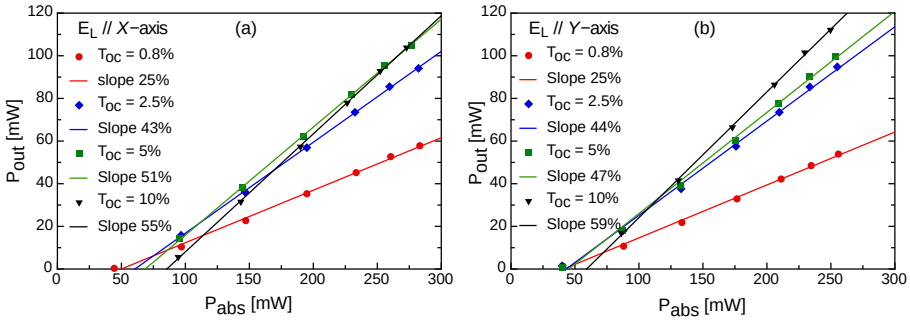

Fig. 3. Laser performance with different OCs in the cw regime for polarization (a) along X-axis and (b) along Y-axis.

In good agreement with the gain cross-section spectra presented in Fig. 2, the emitted output wavelength was around 1060 nm for both crystal orientations, only slightly varying with different OC mirror transitivity. Pump absorption was higher for $E_L \parallel X$-axis crystal orientation, as expected because of the higher value of absorption cross section at the 976 nm pump wavelength for this polarization [6]. Nevertheless, due to the higher emission cross section, the maximum output of 112 mW, was obtained for the $E_L \parallel Y$-axis crystal orientation employing the optimum $T_{oc} = 10\%$ mirror. The corresponding slope efficiency, measured with respect to the absorbed pump power, was 59%. We also carried out a Caird analysis [11], in order to estimate the total round-trip resonator losses δ (reabsorption losses excluded) and the intrinsic slope efficiency η_0, by fitting the measured slope efficiency η as a function of the reflectivity of OC, with the following equation:

$$\eta = \eta_0 \frac{\lambda_p}{\lambda_l} \frac{-\ln(R_{oc})}{\delta - \ln(R_{oc})} \tag{1}$$

where λ_p and λ_l are the pump and laser output wavelength, respectively. The results and the best fit curves are shown in Fig. 4(a). The high values of η_0 obtained for both crystal orientations ($\eta_0 \lesssim 0.7$) suggest a well optimized resonator design and a good crystal quality.

A single fused silica (FS) prism was used for wavelength tuning in cw regime. Employing the $T_{oc} = 0.8\%$ output coupler, a broad tuning range of ~ 50 nm was obtained as shown in Fig. 4(b) for the more promising $E_L \parallel Y$-axis polarization.

Optics EXPRESS

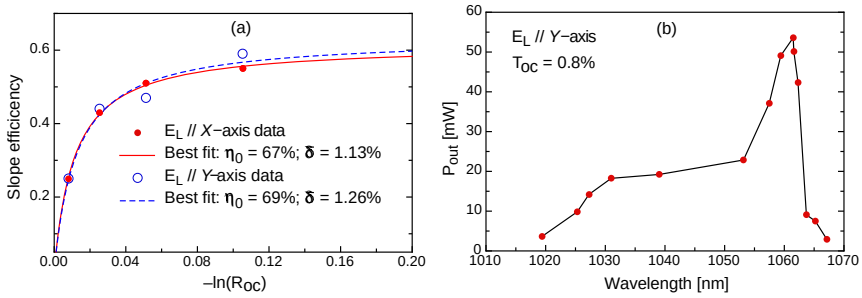

Fig. 4. Slope efficiency as a function of the OC reflectivity for both crystal orientations (a), and output wavelength tuning range in CW regime for the $E_L \parallel Y$-axis crystal orientation.

2.2. *Soliton mode-locking experiments*

For soliton ML experiments, we replaced mirror M_4 (see Fig. 1), with a SESAM specified with a modulation loss $\Delta R = 3\%$ and a saturation fluence $F_{sat} = 140\ \mu J/cm^2$. Intracavity group delay dispersion (GDD) compensation was provided either by GTI mirrors or by a single FS prism [12], as shown in Fig. 1.

Referring to Fig. 1, in the cavity configuration exploiting GTI mirrors, employing either a $T_{oc} = 0.8\%$ or $T_{oc} = 0.4\%$ OC, stable and self-starting soliton ML regime was obtained with a minimum number of 2 bounces per mirror on GTI_2 and GTI_3 and a single bounce on GTI_1, corresponding to a total negative dispersion per round trip of ≈ -4800 fs^2. For $E_L \parallel Y$-axis crystal orientation, shorter pulses were obtained by using a $T_{oc} = 0.4\%$ OC, with a minimum pulse duration of 171 fs and an average output power of 15 mW. The corresponding optical spectrum was centered at 1058 nm with a FWHM of 9 nm, resulting in a time-bandwidth product of 0.41. Slightly longer pulses (~ 200-fs-long) with about 25 mW output power were obtained with $T_{oc} = 0.8\%$ OC.

In order to ease the fine tuning of intracavity GDD and better exploit the available material bandwidth, we tested also a single dispersive prism resonator configuration. To this purpose, we removed the GTI mirrors and inserted a single FS prism at a distance of about 950 mm from the “virtual prism”, whose position calculated through ABCD modeling of the cavity and is close to mirror M_1 (see [12] for a detailed explanation of the oscillator design principles). The maximum negative GDD corresponding to this “virtual”-to-real prism separation was ~ -4500 fs^2 per round trip.

Stable and self-starting ML was readily obtained when the FS prism was hit close to the tip. By finely adjusting the prism insertion we could optimize the amount of negative GDD and minimize soliton pulse duration. The shortest pulse autocorrelation trace and optical spectrum for both possible crystal orientations are shown in Fig. 5.

Employing the $T_{oc} = 0.4\%$ OC, 125-fs-long (FWHM) pulses, assuming a $sech^2$ shaped intensity profile, were obtained for $E_L \parallel Y$-axis crystal orientation, the corresponding optical spectrum was about 12 nm FWHM, centered at 1065 nm, resulting in a time-bandwidth product of 0.4. Only slightly longer pulses (132 fs) were obtained for the polarization $E_L \parallel X$-axis crystal orientation in the same cavity configuration. Pulse train average output power was about 20 mW for both crystal orientations.

The good stability of the ML regime was confirmed by the radio frequency (RF) spectrum of the pulse train. In Fig. 6 we show the fundamental beat note at ~ 117 MHz, with a high extinction ratio of ~ 50 dB, indicating the absence Q-switching instabilities. The RF spectrum in a 1-GHz span with a 10 kHz resolution bandwidth, shown in the inset of Fig. 6, is also indicative of clean single-pulse operation of the laser.

Optics EXPRESS

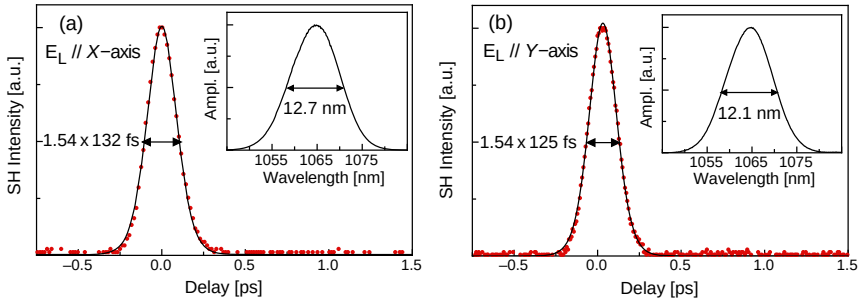

Fig. 5. Autocorrelation trace and corresponding optical spectrum (insets) of the shortest pulses obtained in single FS prism resonator configuration for (a) $E_L \parallel X$-axis and (b) $E_L \parallel Y$-axis Yb:$MgWO_4$ crystal orientation.

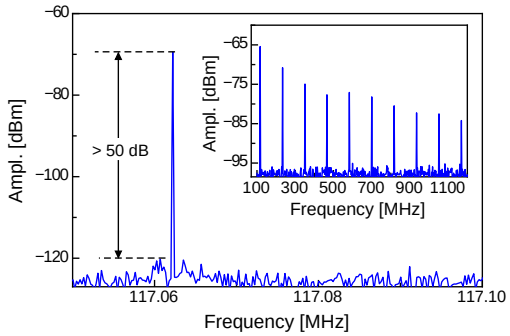

Fig. 6. RF spectrum of the cw ML pulse train at the fundamental beat note and (inset) with 1 GHz span for the $E_L \parallel Y$-axis Yb:$MgWO_4$ crystal orientation. Very similar results were obtained also for the $E_L \parallel X$-axis crystal orientation.

3. Conclusions

In conclusion, we presented a detailed performance characterization of a single-mode diode-pumped Yb:$MgWO_4$ laser. For both $E_L \parallel X$-axis and Y-axis crystal orientations, we demonstrated low-threshold cw operation, with high intrinsic slope efficiency and, for the first time to the best of our knowledge, femtosecond pulse generation in a SESAM soliton ML oscillator. Pulses as short as 125 fs where obtained for the $E_L \parallel Y$-axis crystal orientation and only slightly longer (132 fs) for $E_L \parallel X$-axis. A better optimized combination of a shorter crystal with higher doping could easily lead to a further improvement of this already promising performance in the ML regime, fully exploiting the advantages of high-brightness, low-power single mode diodes. In addition, the good thermal properties of $MgWO_4$ and the relatively broad absorption peak centered at 976 nm, are favorable properties for a significant power scaling with this promising novel laser material.

Funding

The National Natural Science Foundation of China (No.11404332, No.61575199); Key Project of Science and Technology of Fujian Province (2016H0045); the Strategic Priority Research Program of the Chinese Academy of Sciences (No.XDB20000000); the Instrument Project of Chinese Academy of Sciences (YZ201414); and the China Scholarship Council (CSC, No.201504910418 and No. 201504910629).